Megasonic cleaning, cavitation, and substrate damage: an atomistic approach

Kapila, Vivek, Deymier, Pierre, Shende, Hrishikesh, Pandit, Viraj, Raghavan, Srini, et al.

Vivek Kapila, Pierre A. Deymier, Hrishikesh Shende, Viraj Pandit, Srini Raghavan, Florence O. Eschbach, "Megasonic cleaning, cavitation, and substrate damage: an atomistic approach," Proc. SPIE 6283, Photomask and Next-Generation Lithography Mask Technology XIII, 628324 (20 May 2006); doi: 10.1117/12.681771

SPIE.

Event: Photomask and Next Generation Lithography Mask Technology XIII, 2006, Yokohama, Japan

Megasonic cleaning, cavitation, and substrate damage: an atomistic approach

Vivek Kapila[a], Pierre A. Deymier[a], Hrishikesh Shende[a], Viraj Pandit[b], Srini Raghavan[a] and Florence O. Eschbach[c]

[a]Department of Materials Science & Engineering, University of Arizona, Tucson, AZ 85721;
[b]Department of Electrical & Computer Engineering, University of Arizona, Tucson, AZ 85721;
[c]Intel Corporation, California Technology & Manufacturing Group, Santa Clara, CA 95054

ABSTRACT

Megasonic cleaning has been a traditional approach for the cleaning of photomasks. Its feasibility as a damage free approach to sub 50 nm particulate removal is under investigation for the cleaning of optical and EUV photomasks. Two major mechanisms are active in a megasonic system, namely, acoustic streaming and acoustic cavitation. Acoustic streaming is instrumental in contaminant removal via application of drag force and rolling of particles, while cavitation may dislodge particles by the release of large energy during cavity implosion or by acting as a secondary source of microstreaming. Often times, the structures (substrates with or without patterns) subjected to megasonic cleaning show evidence of damage. This is one of the impediments in the implementation of megasonic technology for 45 nm and future technology nodes. Prior work suggests that acoustic streaming does not lead to sufficiently strong forces to cause damage to the substrates or patterns. However, current knowledge of the effects of cavitation on cleaning and damage can be described, at best, as speculative. Recent experiments suggest existence of a cavity size and energy distributions in megasonic systems that may be responsible for cleaning and damage. In the current work, we develop a two-dimensional atomistic model to study such multibubble cavitation phenomena. The model consists of a Lennard-Jones liquid which is subjected to sinusoidal pressure changes leading to the formation of cavitation bubbles. The current work reports on the effects of pressure amplitude (megasonic power) and frequency on cavity size distributions in vaporous and gaseous cavitation. The findings of the work highlight the role of multibubble cavitation as cleaning and damage mechanism in megasonic cleaning.

Keywords: Photomask cleaning, Megasonics, Cavitation.

1. INTRODUCTION

The progress in the semiconductor industry has historically been made possible by the advances made in the optical lithography. Until recently, dry and transmissive lithographic techniques have been successful in printing the ever shrinking feature sizes (currently 65 nm) on the silicon wafer. However, current lithography methods appear to have reached a limit where they will not be suitable in printing of future technology nodes (45 nm, 32 nm). Immersion and EUV are the competing lithography technologies for 32 nm and EUV lithography is considered to be the enabler technology at the 22 nm node. EUV lithography will employ light of 13.4 nm wavelength. At this wavelength, light is absorbed by most materials. Therefore, highly reflective photomasks made of multiple layers of Si and Mo are being developed for the transfer of patterns on the Si wafer.[1] One of the major challenges in the implementation of EUV technology is the fabrication of defect free masks. The EUV photomasks are expected to have zero defects of size above 30 nm. Therefore, cleaning of the EUV photomasks is a critical step in the future manufacturing. Not only the cleaning method should be able to remove particles with high efficiency to size down to 30 nm but it should also be damage free. Megasonic cleaning has been one of the most successful approaches in the cleaning of wafers and photomasks. This is a wet cleaning process in which sound wave at a frequency of 1 MHz or above is sent in the cleaning fluid (aqueous solution).[2] The sound wave in the fluid travels as a pressure wave[3] and gives rise to several physical phenomena, namely acoustic streaming

Further author information: (Send correspondence to V. Kapila)
V. Kapila.: E-mail: vkapila@email.arizona.edu, Telephone: 1 520 626 8997

Photomask and Next-Generation Lithography Mask Technology XIII, edited by Morihisa Hoga,
Proc. of SPIE Vol. 6283, 628324, (2006) · 0277-786X/06/$15 · doi: 10.1117/12.681771

and acoustic cavitation. Acoustic streaming is motion of fluid caused by the attenuation of sound wave traveling in the viscous fluid.[4, 5] Acoustic cavitation is formation of vaporous/gaseous bubbles in the cleaning fluid during the low pressure cycle of propagating acoustic wave, followed by violent implosion during high pressure cycle of the acoustic wave.[6]

Both acoustic streaming and cavitation are believed to play important roles in the megasonic cleaning of wafer and photomask surfaces. Acoustic streaming has been shown to reduce the thickness of the hydrodynamic boundary layer at the solid-fluid interface. This exposes the particles adhered to the surfaces to large velocity gradients in the flow (Schlichting streaming) in a thin acoustic boundary layer.[7] Therefore, under appropriate conditions of megasonics, sufficiently large drag force and rolling moments can be obtained to overcome adhesion force between particles and surface leading to removal by rolling and sliding of particles.[8] In the case of cavitation, stable and transient bubbles are believed to exist in the fluid.[6] Stable bubbles oscillate about an equilibrium radius and these bubbles act as secondary sound sources and can give rise to microstreaming. The transient bubbles are short lived and during high pressure cycle of the acoustic wave, these bubbles undergo a violent implosion. The implosion of bubbles results in extreme conditions of pressure and temperature and may give rise to shock waves. Also, near a solid boundary the implosion of bubbles is shown to be asymmetric and may result in a fluid jet. Both microstreaming and shock waves resulting from cavitation can be instrumental in dislodging the particles adhered to the surfaces.

Often times, megasonic cleaning has also been associated with the damage observed on the cleaned surfaces.[9] While megasonic cleaning has advantages over many other cleaning technologies in terms of particle removal efficiency (PRE), the issue of damage is becoming one of central importance considering the fragility of patterns owing to their small sizes.[10] It is extremely difficult to gain a complete understanding, in an experimental set up, of the primary mechanisms at play in cleaning and damage as many complex processes are operative at any given time. Theoretical approaches provide effective means of investigating the effects of various cleaning mechanisms separately. In a previous work we have reported on the role of acoustic streaming in the particle removal using a continuum simulation approach.[8] The conditions required for particle removal by acoustic streaming were identified. The current work focuses on gaining a better fundamental understanding of cavitation phenomena in megasonic cleaning.

Cavitation has long been investigated in many diverse areas of science and engineering using continuum approaches.[6] However, these continuum models have been essentially limited to studies of single bubble cavitation and usually can not predict bubble dynamics just before and after the implosion. It has been recognized in recent experimental studies that megasonic cleaning is a multibubble phenomena and there exists a distribution of bubble sizes and energies that may be responsible for particle removal and damage.[11] Owing to the inherent limitations of the continuum approaches in investigating such multibubble phenomena we choose to use an atomistic simulation approach. Specifically, we use molecular dynamics simulations to study the effects of frequency and power of megasonics on vaporous and gaseous cavitation and cavity size distributions. The paper is organized as follows, in section 2 we present the atomistic model used in this work, this is followed by the results and discussion in section 3, finally the findings of the work are summarized in section 4.

2. MODEL AND METHODS

In the present work, two-dimensional simulations are performed using the method of molecular dynamics (MD) to study acoustic cavitation in megasonic cleaning systems. In contrast to continuum simulations, where the physical system is studied as a continuous media, in MD simulations the system is composed of individual atoms or molecules. The interaction between the atoms of the system is described by a potential function $V(r)$ where r is the distance between a pair of atoms. In the current work, the fluid medium is modeled as a Lennard-Jones (LJ) system in which the interactions between pairs of atoms are described by,

$$V_{ij}(r) = 4\epsilon((\frac{\sigma_{ij}}{r_{ij}})^{12} - (\frac{\sigma_{ij}}{r_{ij}})^{6}), \tag{1}$$

where $V_{ij}(r_{ij})$ is the potential energy of the pair of atoms "ij", and ϵ and σ are the LJ parameters that describe, respectively, the energy and separation between a pair of atoms at equilibrium. Fig. 1 shows the

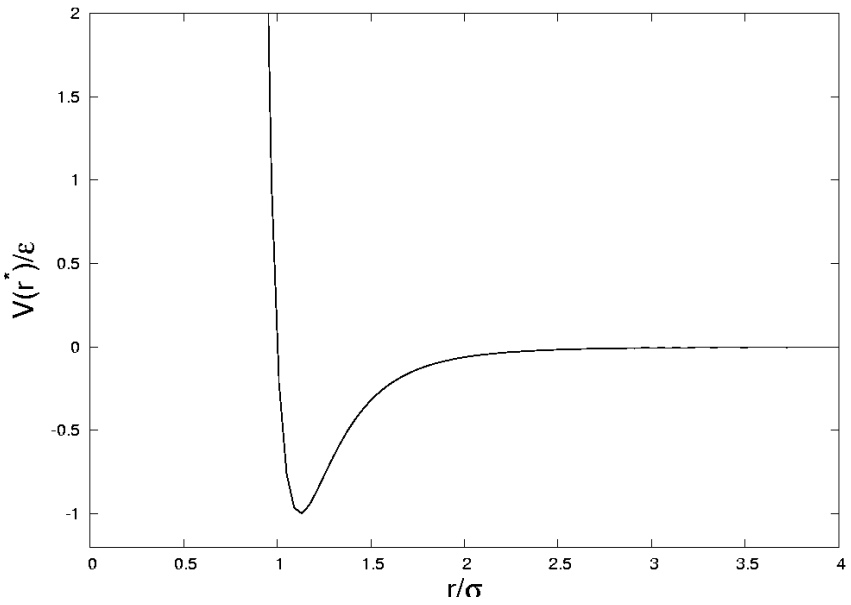

Figure 1. Illustration of LJ potential.

potential function V as a function of distance between atomic pair, r. As seen in Fig. 1, LJ potential captures the most essential physics of interaction between atoms in a physical system, i.e., attraction between the atoms when they are far apart, a minimum in the potential function at equilibrium, and repulsion at small distances. The choice of parameters ϵ and σ depends on the physical medium to be simulated.

For the sake of simplicity, in MD simulations, physical quantities such as pressure, temperature, and density, etc. are often represented in terms of the reduced units. For example, considering ϵ and σ as units of energy and length, respectively, relationship between the real and reduced unit representation of physical quantities is described as,

$$\begin{aligned} r^* &= r/\sigma, \\ \rho^* &= N\sigma^n/V, \\ P^* &= P\sigma^n/\epsilon, \\ T^* &= k_{\mathrm{B}}T/\epsilon \end{aligned} \tag{2}$$

where N is the number of atoms, ρ is the number density, P is the pressure, T is the temperature, V is the volume, and $\mathrm{k_B}$ is the Boltzmann constant. The quantity n represents the dimensionality of the simulated system. Because of computational limitations, we investigate two-dimensional systems, here $n = 2$. The asterisks in the subscripts represent the physical quantity in reduced units. The time evolution of the system is followed by solving Newtons equations of motion of each individual atom given by

$$\begin{aligned} \dot{\mathbf{r}}_i &= \frac{\mathbf{p}_i}{m}, \\ \dot{\mathbf{p}}_i &= F_i \end{aligned} \tag{3}$$

where $\mathrm{p_i}$ is the momentum, m is the mass, r is the position of atom i, and a dot over a quantity represents its time derivative. The equations of motion (3) are integrated using Verlet's method[12] based on a finite difference approach as follows,

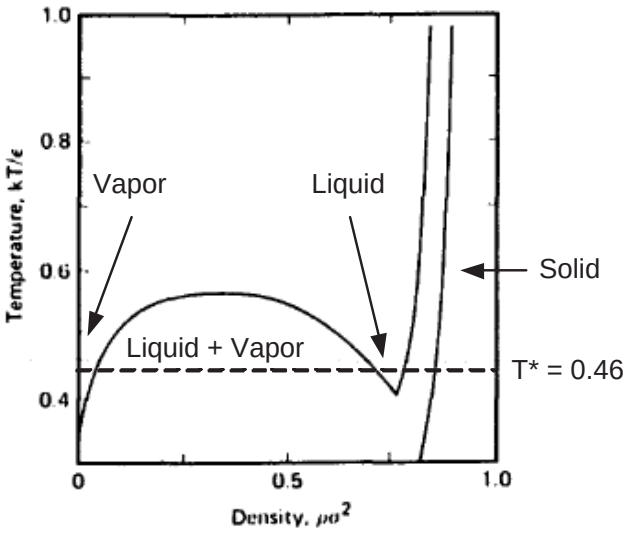

Figure 2. Phase diagram for 2-D Lennard-Jones system.

$$\begin{aligned} r_i(t+\Delta t) &= 2r_i(t) - r_i(t-\Delta t) + \frac{F_i}{m}t^2, \\ \dot{r_i} &= \frac{r_0(t+\Delta t) - r_0(t-\Delta t)}{2\Delta t} \end{aligned} \tag{4}$$

where Δt is the time step.

The starting structure in a MD simulation is often generated by placing the atoms on a lattice and then brought to the desired conditions of pressure and temperature etc. by heating and expanding the simulation cell. This prevents any instability in the numerical calculations because of any potential overlap of atomic positions. In the present work, the simulation box consists of 26672 LJ atoms. The starting configuration is obtained by placing atoms on a triangular lattice at a reduced density of 1.0 and at a reduced temperature of 0.4. The phase diagram of the two-dimensional LJ system is shown in Fig. 2. It is seen from Fig. 2 that pure LJ liquid exists at $T^* = 0.46$ and $\rho^* = 0.75$. Therefore, temperature of the system is slowly increased to 0.46. This is followed by an expansion of the simulation cell to a reduced density of 0.75.

The temperature and pressure of the LJ fluid are maintained at the desired value by application of a Nose-Hoover thermostat and an Andersen barostat.[12] The thermostat and barostat introduce additional, artificial degrees of motion in the equations of motion (3). The inertia associated with the barostat degree of freedom is determined by a series of simulation of the liquid such that the relaxation time of the volume of the simulation cell approaches the time for a sound wave to propagate across the simulated system, namely L/v_{sound} where L is the length of the edge of the simulation cell and v_{sound} is the speed of sound in the fluid. The inertia associated with the thermostat is chosen to be small in order to impose good isothermal conditions. Note that a large thermal inertia can also be employed if one is interested in investigating cavitation under adiabatic conditions.

3. RESULTS AND DISCUSSION

3.1. Vaporous Cavitation

We have investigated the process of multibubble cavitation in a two-dimensional pure Lennard-Jones liquid (Argon). The Lennard-Jones potential parameters for this element are $\sigma = 3.405$ Å and $\epsilon/k_{\rm B} = 119.8\ ^0$K where

k_B is Boltzmann constant. Under the assumption that the pressure of a passing acoustic wave is uniform over the scale of our small atomistic system, the effect of the acoustic wave on the liquid is mimicked by applying onto the simulation cell an external pressure varying sinusoidally with time, t, given by

$$P(t) = P_e - P_a \mathrm{Sin}(2\pi\nu t), \tag{5}$$

where P_e is the equilibrium pressure of the liquid at the initial temperature and density studied and P_a is the amplitude of the sinusoidal pressure. The temperature of the two-dimensional argon liquid is $\sim 55\ ^0$K ($T^* = 0.46$), with an initial two-dimensional atomic density of 0.0629 atom/Å^2 (the total number of atoms in the simulated system is 26672 in a two-dimensional cell 65.13×65.13 nm^2). At this density and temperature the equilibrium pressure of the liquid is 4.734×10^{-3} N/m ($P^* = 0.332$). The frequency of the sinusoidal pressure, ν, is chosen to take the values, 77, 116, 154, and 232 MHz. This choice of high frequencies is imposed by the method of molecular dynamics that necessitates a very small time step for integrating numerically in time the equations of motion of each individual atom. The time step, Δt, for this liquid is 2.156×10^{-15} sec. In terms of time integration steps, the frequencies applied in this study correspond to periods of 6, 4, 3, and $2 \times 10^6 \Delta t$ which represent very long molecular dynamics simulations.

The results of a typical simulation are reported in Fig. 3 for a frequency of 154 MHz and a pressure amplitude $P_a = 0.084 P_e$. Fig. 3(a) shows the first half of the sinusoidal cycle during which the external pressure lies below the equilibrium pressure (dotted line). The solid line in Fig. 3(a) shows the variation of the internal pressure of the liquid that tries to balance the externally applied pressure. The internal pressure exhibits additional oscillations on a shorter time scale that correspond to the natural frequency of the simulated system (the period of these oscillations are related to the artificial inertia of the volume degree of freedom used in the Andersen's constant pressure MD method). These oscillations are also clearly seen in the time variation of the two-dimensional volume (area) of the simulated system shown in Fig. 3(b). Note that as the external pressure and consequently the internal pressure of the system drop below the equilibrium pressure of the liquid, the increase in volume takes the density of the liquid inside a two-phase region of stability leading to the coexistence of a liquid with a vaporous phase. The transformation of the liquid into the vaporous phase results in the formation of vaporous cavities in the liquid. In addition to volume and pressure, we also monitor the temperature of the system (see Fig. 3(c)). Since the simulation is conducted under isothermal conditions by interfacing the atomistic system to a Nose-Hoover thermostat, the temperature fluctuates only marginally by approximately 1 ^{0}K. The total energy of the simulated system is reported in Fig. 3(d). As anticipated, the energy increases during the expansion phase of the pressure wave.

In order to monitor the process of formation of vaporous cavities, we have discretized the two-dimensional system into subcells 9.19×9.19 Å^2 and recorded the atomic density inside each subcell. These maps of atomic density are then employed to locate and identify the cavities. A subcell containing less than 5 atoms is considered to be representative of the vaporous phase while a subcell with more than 5 atoms is filled with liquid phase. We conduct a statistical analysis of the diameter of the cavities present in the system. In this statistical analysis, we have disregarded the cavities with a radius less than 23 Å which are also commonly observed in the liquid at the equilibrium pressure. By discarding the very small cavities that may be associated with local density fluctuations in the equilibrium liquid, we investigate only the effect of the sinusoidal pressure on the system.

In Fig. 4, we see that as the liquid expands, the number of cavities with diameters exceeding 23 Å increases. The average cavity diameter at the apex of expansion exceeds 40 Å. However, and more importantly, the standard deviation of the cavity diameter also increases with expansion. At the maximum expansion, the distribution of cavity diameters is broad with some cavities possessing diameters approaching 80 Å. As the external pressure increases during the compression phase of the sonic cycle, the number of cavities decreases as well as their radius. For external pressures exceeding the equilibrium pressure the liquid density increases. We have not completed the sonic cycle at high pressure, since according to the phase diagram of the two-dimensional Lennard-Jones liquid, at high pressure the liquid will crystallize. This high-pressure solidification is not encountered in aqueous based liquids subjected to sonic irradiation since the solid phase of water is less dense than the liquid phase. This unique feature of water makes the comparison between the liquid Lennard-Jones system and water impossible in the compressive stage of the sonic cycle. We therefore limit all our studies to the expansion period of that

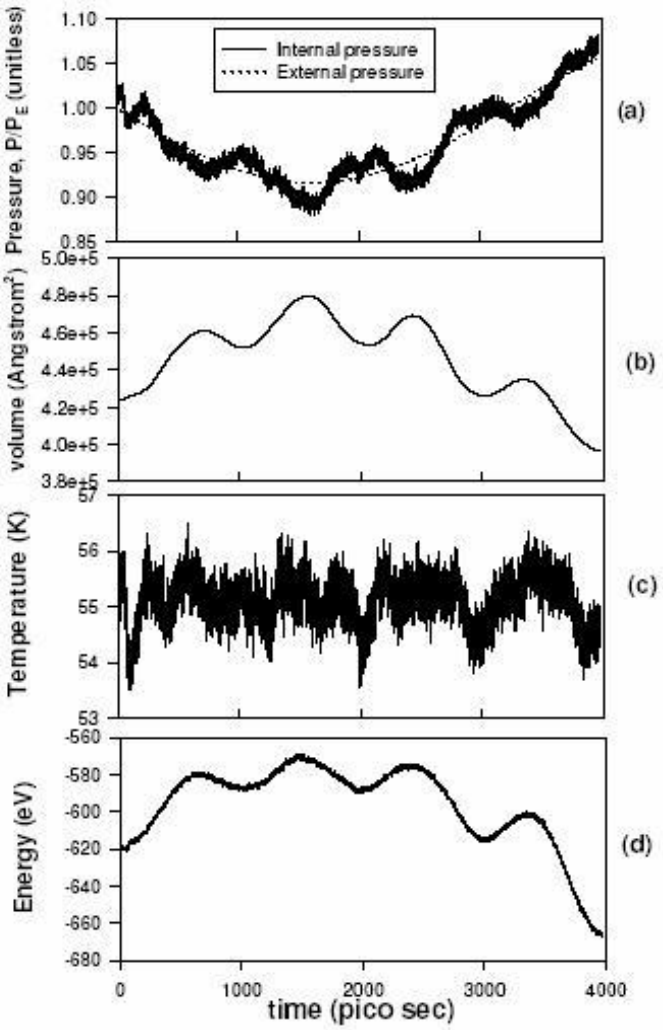

Figure 3. Time evolution of the external and internal pressure, volume, temperature and energy of the liquid subjected to a sinusoidal pressure with a frequency of 154 MHz, and pressure amplitude 0.084 P_e.

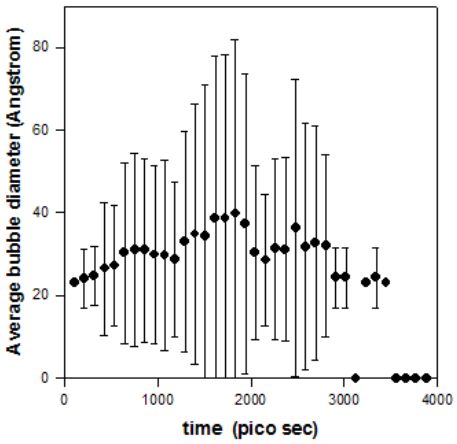

Figure 4. Time evolution of the average cavity size and standard deviation for the liquid subjected to a sinusoidal pressure with a frequency of 154MHz, and pressure amplitude $0.084P_e$.

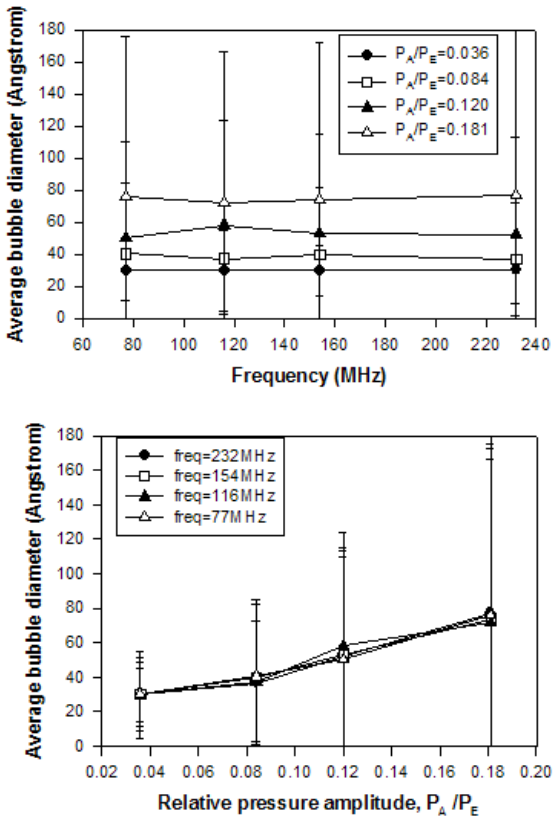

Figure 5. Average cavity diameter and standard deviation versus (a) frequency and (b) pressure amplitude.

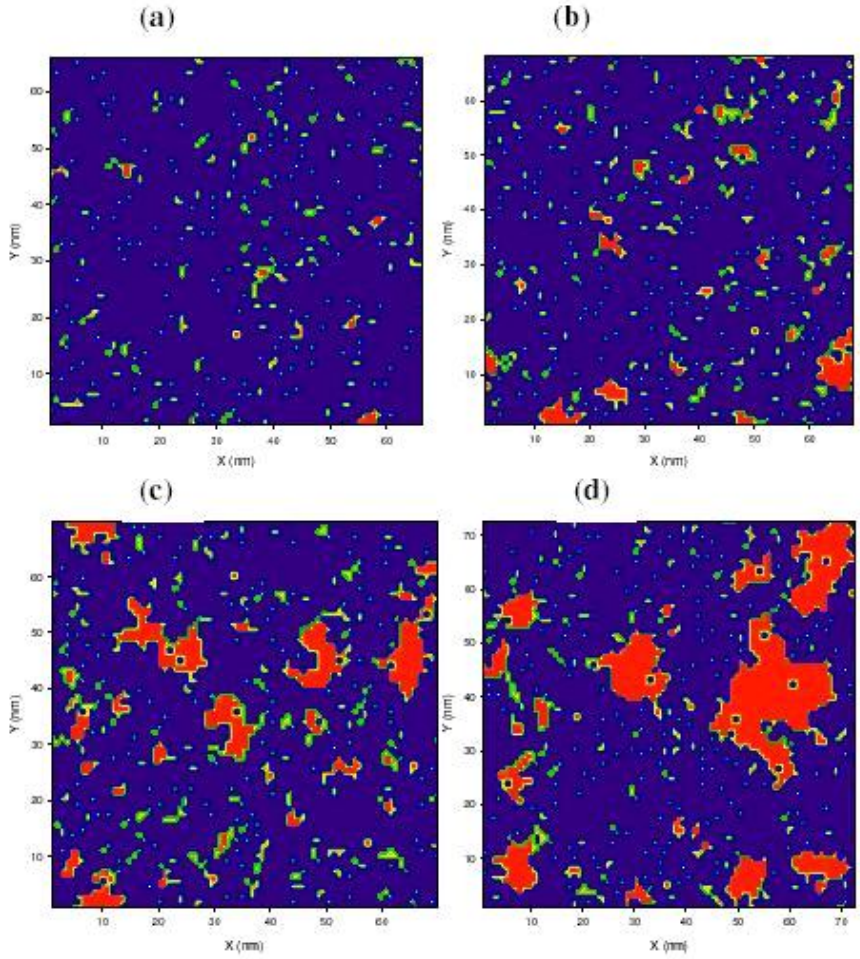

Figure 6. Snapshots of the liquid subjected to a sinusoidal pressure with a frequency of 77 MHz, and pressure amplitude (a) 0.036, (b) 0.084 , (c) 0.120, and (d) 0.180 P_e.

cycle. The average cavity diameter and standard deviation at maximum volume expansion for all the pressure amplitudes and frequencies studied are presented in Fig. 5 (a) and (b).

It is noted that for all pressure amplitudes, the average cavity diameter and diameter standard deviation are independent of frequency. In contrast, as the pressure amplitude increases, the average cavity diameter increases as does the standard deviation. This suggests that during vaporous cavitation, at the minimum pressure (maximum volume expansion), the cavity size increases and the cavity size distribution widens.

Fig. 6 (a)-(d) show the gaseous phase (red) and liquid phase (blue) at maximum expansion for the lowest frequency (77 MHz) at the four pressure amplitude studied. As the pressure amplitude increases, the cavity size increases. Note, however, that the total number of cavities at the largest pressure amplitude seem to have dropped suggesting that coalescence of cavities may be taking place. This evolution will be contrasted in more details to that of gaseous cavitation presented in the next section.

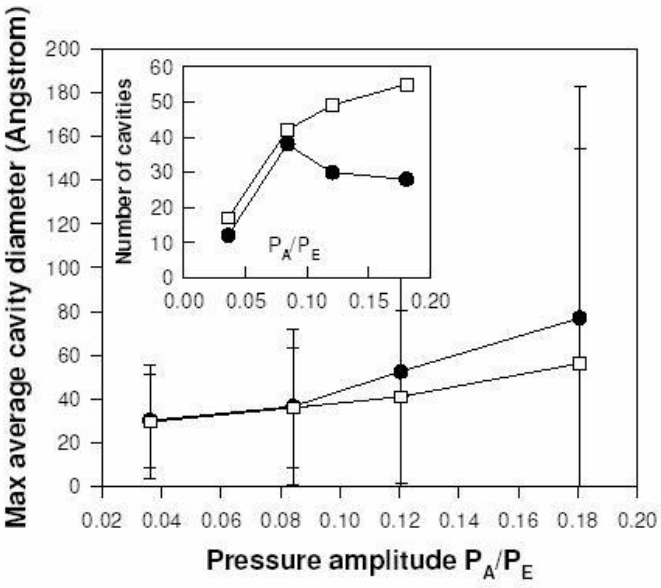

Figure 7. Average cavity diameter and standard deviation versus relative pressure amplitude in the case of vaporous cavitation (filled symbol) and gaseous cavitation (open symbol). The gas content is 10 atomic percent. The frequency of the sinusoidal pressure is 232 MHz. The inset shows the number of cavities versus relative pressure amplitude.

3.2. Gaseous Cavitation

Here we investigate the phenomenon of cavitation in a fluid containing a dissolved gas. Again the liquid is Ar and the dissolved gas is Ne. The parameters for the Ar-Ar LJ interactions are the same as before. The parameters for the Ne-Ne interactions are $\sigma = 2.780$ Å and $\epsilon/k_{\rm B} = 34.9\ ^0$K. Simulations of mixtures require also interactions between Ar and Ne atoms. The LJ parameters for this type of interaction are $\sigma = 3.0925$ Å and $\epsilon/k_{\rm B} = 35.9\ ^0$K. The parameter $\sigma_{\rm Ar-Ne}$ is the arithmetic average of the parameters for the pure substances. The energy parameter is chosen to be on the order of that of Ne to favor gas dissolution. A series of simulations of Ar liquids containing various concentrations of gas, namely 2.5, 5, 10 and 20 Ne atomic % are conducted for frequencies and pressure amplitudes of the externally applied sinusoidal pressure identical to those of the pure liquid. We first contrast the behavior of the gaseous system and the vaporous system in Fig. 7. The presence of gas dissolved in the liquid impacts the average diameter of cavitations as well as the distribution of cavity diameter. At high pressure amplitude, the dissolve gas favors smaller cavities with a narrower diameter distribution. It is worthy noting that as the pressure amplitude increases the excess volume of the gaseous system is accommodated by a monotonously increasing number of small cavities. This behavior differs significantly from the vaporous cavitation process which exhibits a decreasing number of large cavities (forming via coalescence) beyond some pressure amplitude.

The morphology of the expanded liquid containing dissolved gases is clearly illustrated in Fig. 8. At the highest pressure amplitude the system is composed of numerous small gas filled cavities. This behavior should be compared to that of the vaporous cavitation illustrated in Fig. 6.

The effect of gas content of cavitation is summarized in Fig. 9 and illustrated in Fig. 10. We note that the largest cavities form at low gas concentrations. At and above 5% concentration, the cavitation process is dominated by the formation of numerous small gaseous cavities with a diameter distribution narrower than that of the low concentration cases.

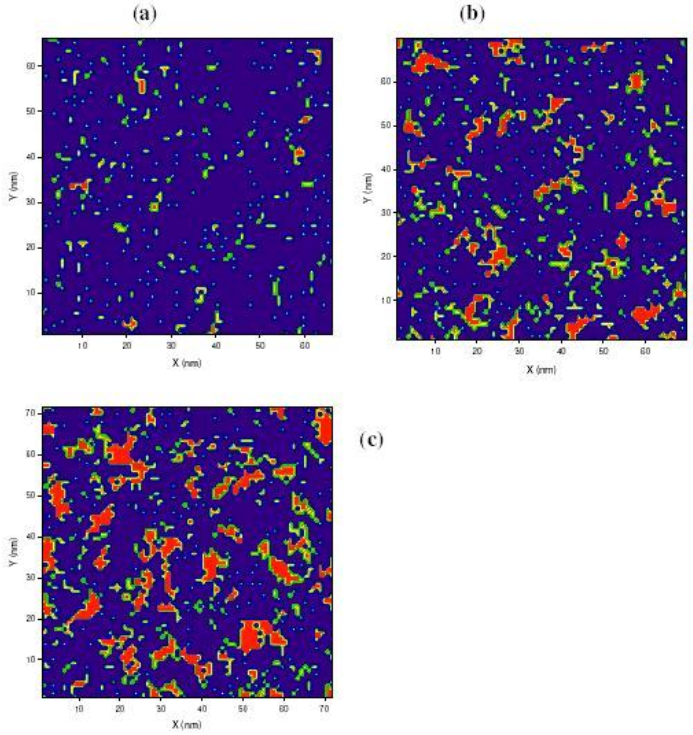

Figure 8. Snapshots of the gaseous liquid subjected to a sinusoidal pressure with a frequency of 77MHz, and pressure amplitude (a) 0.036, (b) 0.120, and (c) 0.180 P_e. The gas content is 10 atomic percent.

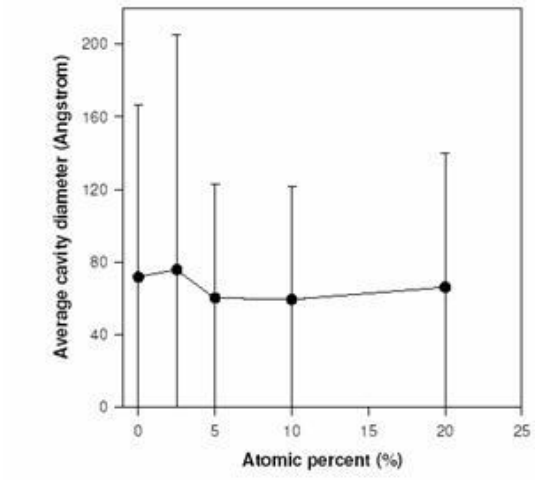

Figure 9. Average cavity diameter and standard deviation versus gas content. The frequency of the sinusoidal pressure is 116 MHz. The pressure amplitude is $0.18P_e$.

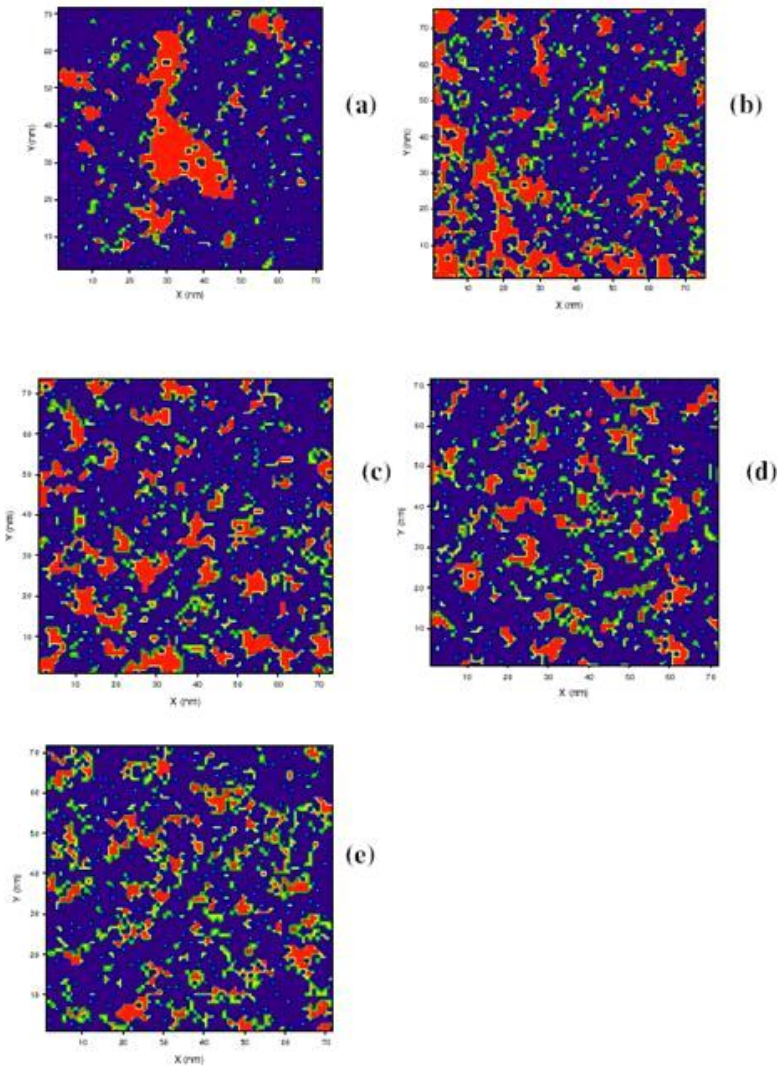

Figure 10. Snapshots of the gaseous liquid subjected to a sinusoidal pressure with a frequency of 116 MHz, and pressure amplitude 0.180 P_e. The gas content is (a) 0%, (b) 2.5%, (c) 5%, (d) 10% and (e) 20%.

4. CONCLUSIONS

We have developed a simple atomistic model of a liquid that can be subjected to sinusoidal external pressure to study the phenomenon of cavitation. We have investigated the phenomena of vaporous and gaseous multibubble cavitation. Vaporous cavitation leads to the formation of large cavities in contrast to the process of gaseous cavitation. Even though we have not considered here the behavior of cavities under the compressive phase of a sonic cycle, we expect that large cavities will lead to significantly higher concentration of energy upon compression. This result is consistent with the common experimental observation of more violent cavitation processes (e.g. sonoluminescence) in degassed fluids as compared to fluids containing dissolved gases. The effect of acoustic power density on cavitation is illustrated here by the effect of pressure amplitude of the applied sinusoidal pressure. Increases in pressure amplitude drastically increase the size of vaporous cavities while this effect is significantly reduced by the presence of dissolved gases. Because of computational limitations, we have restricted our simulations to high frequencies. However, our calculations seem to indicate that frequency impacts the formation of cavities to a lesser extent than pressure amplitude. Of course, our calculations are limited to one acoustic cycle and do not account for cavity growth via rectified diffusion.

Our work stresses the importance of multibubble cavitation in understanding the process of megasonic cleaning. In particular we emphasize an understanding of the distribution of cavity size. We believe that control of this distribution may lead to cavitation-driven megasonic cleaning processes that can maximize cleaning efficiency and minimize underlying events that can damage structures.

The simulations in the current work have been limited to the expansion phase of sonic cycle. Future work will involve modeling of non-LJ systems that may allow studies during compression phase of acoustic wave. This will enable simulations of rectified diffusion and its effect on cavitation. The focus will be on compression phase transfer of energy from bubble implosions to the nearby substrate. The effect of multiple chemistries and systems with dissolved gases will be investigated. Specifically, the model will be expanded to evaluate the effect of viscosity (chemistry) and thermal conductivity of gases on cavitation process.

REFERENCES

1. G. Stix, "Getting more from moore's," *Scientific American* **284**, p. 32, 2001.
2. A. A. Busnaina, I. I. Kashkoush, and G. W. Gale, "An experimental-study of megasonic cleaning of silicon-wafers," *J. Electrochem. Soc.* **142**, p. 2812, 1995.
3. R. Resnick and D. Halliday, *Physics*, Wiley, NewYork, 1990.
4. D. Zhang, *Fundamental study of megasonic cleaning*. PhD thesis, University of Minnesota, 1993.
5. W. L. Nyborg, "Acoustic streaming," in *Physical Acoustics - Vol. II B*, W. P. Mason, ed., pp. 265–331, Academic, London, 1965.
6. F. R. Young, *Cavitation*, McGraw-Hill, London, 1989.
7. H. Schlichting, *Boundary-Layer Theory*, McGraw-Hill, NewYork, 1968.
8. V. Kapila, P. A. Deymier, H. Shende, V. Pandit, S. Raghavan, and F. O. Eschbach, "Acoustic streaming effects in megasonic cleaning of euv photomasks: A continuum model," in *25th Annual BACUS Symposium on Photomask Technology*, J. T. Weed and P. M. Martin, eds., *Proc. SPIE* **5992**, pp. 59923X–1, 2005.
9. F. Holsteyns, A. Riskin, G. Vereecke, A. Maes, and P. M. Mertens *Electrochemical Society* **PV-26**, 2003.
10. A. Hand, "Damage free cleaning beyond 65 nm," *Semiconductor International* **Jan. 2005**.
11. F. Holsteyns, K. Lee, S. Graf, R. Palmans, G. Vereecke, and P. W. Mertens, "Megasonics: A cavitation driven process," *Solid State Phenomena* **103-104**, 2005.
12. M. Allen and D. Tildesley, *Computer Simulation of Liquids*, Clarendon Press, Oxford, 1987.